Journal of Power Sources 263 (2014) 125–129

Contents lists available at ScienceDirect

Journal of Power Sources

journal homepage: www.elsevier.com/locate/jpowsour

Short communication

$La_{1.6}Sr_{0.4}NiO_4$ one-dimensional nanofibers as cathode for solid oxide fuel cells

Qiang Li [a], Liping Sun [a], Hui Zhao [a,*], Hailong Wang [a], Lihua Huo [a], Aline Rougier [b], Sébastien Fourcade [b], Jean-Claude Grenier [b]

[a] Key Laboratory of Functional Inorganic Material Chemistry, Ministry of Education, School of Chemistry and Materials Science, Heilongjiang University, Harbin 150080, PR China
[b] CNRS, Université de Bordeaux, ICMCB, 87 avenue du Dr. A. Schweitzer, F-33608 Pessac-Cedex, France

HIGHLIGHTS

- $La_{1.6}Sr_{0.4}NiO_4$ nanofibers cathode is studied for applications in SOFCs.
- Nanofibers cathode gave the lowest polarization resistance of 0.40 Ω cm^2 at 700 °C.
- The rate limiting step for oxygen reduction reaction is the charge transfer process.

ARTICLE INFO

Article history:
Received 18 December 2013
Received in revised form
7 April 2014
Accepted 8 April 2014
Available online 18 April 2014

Keywords:
Solid oxide fuel cells
Nanofibers cathode
Oxygen reduction reaction
Electrospinning

ABSTRACT

$La_{1.6}Sr_{0.4}NiO_4$ (LSN) nanofibers are prepared by electrospinning technique and used as cathode materials for solid oxide fuel cells (SOFCs) with $Ce_{0.9}Gd_{0.1}O_{1.95}$ (CGO) as electrolyte. The as-prepared cathode is highly porous but forms a good contact with the CGO electrolyte after rapid sintering at 900 °C for 15 min in air. The electrode performance of LSN nanofibers is measured at various temperatures and under different oxygen partial pressures. Two main oxygen reduction reaction (ORR) processes are identified. The rate limiting step for the ORR is the charge transfer process. The LSN nanofiber cathode exhibits a polarization resistance (R_p) of 0.40 Ω cm^2 at 700 °C in air, 0.80 Ω cm^2 at 650 °C and 1.59 Ω cm^2 at 600 °C. These results demonstrate that the LSN nanofiber architecture significantly enhances the electrochemical activity of these cathodes for the ORR compared to usual porous electrodes, which points out the interest of such a synthesis technique for preparing SOFCs cathode materials with peculiar morphology.

1. Introduction

Research on novel electrode materials is one of the critical issues in the development of new generation of solid oxide fuel cells (SOFCs) [1,2]. Cathodes based on nanostructured (including nanoparticles, nanotubes, nanorods and nanofibers) mixed ionic-electronic conductors (MIEC) have great potential for increasing the triple phase boundary (TPB) length and significantly enhance the SOFC performances [3–5].

In recent years, the use of one-dimensional (1-D) nanostructures, including nanotubes and nanofibers, for designing cathode materials in SOFCs has been the subject of intense research due to the reduction of device dimensions [6,7].

It is postulated that the one-dimensional (1-D) nanofiber cathode has several advantages: (1) high porosity; (2) continuous pathway for charge transport; (3) suppression of the grain growth of the matrix by dispersed particles with relatively high sintering temperatures; (4) release of stresses by thermal expansion within the fibers, and (5) excellent scaffold for infiltration.

Bellino et al. prepared $La_{0.6}Sr_{0.4}CoO_3$ nanotubes and realized a new architectured cathodes for SOFCs which show impressively low polarization resistance at intermediate temperatures [8]. Further study indicated that the cathode performance was improved when the nanotubes have sufficiently small diameter to become dense after sintering [9]. Dong et al. fabricated $Sm_{0.5}Sr_{0.5}CoO_3$ nanofiber cathodes by using eggshell membranes (ESMs) as template and studied the electrode properties. It was found that the nanofiber

* Corresponding author.
E-mail address: zhaohui98@yahoo.com (H. Zhao).

http://dx.doi.org/10.1016/j.jpowsour.2014.04.025
0378-7753/

cathode had highly porous interconnectivity and small polarization resistance at low operating temperatures (500–600 °C) [10,11].

Electrospinning technique is an easy, versatile and effective way to prepare nanoscale ceramic fibers and has been used to fabricate nanostructured electrodes of SOFCs [12–15]. For example, a high performance SOFC composite cathode was obtained by infiltrating YSZ nanofiber scaffold with $La_{0.8}Sr_{0.2}MnO_3$ materials [13]. On the other hand, $La_{0.58}Sr_{0.4}Co_{0.2}Fe_{0.8}O_3$ nanofibers have not only large surface-to-volume ratio and high catalytic activity, but also high charge mobility and good thermal stability, due to their 1-D nanostructure [14]. The double-layered perovskite oxide $GdBaCo_2O_{5+\delta}$ was also prepared as nanofibers by electrospinning method and further studies indicated that the nanofiber cathodes exhibited fast oxygen transport and high electrochemical catalytic activity at intermediate temperatures [15]. Recently, we prepared $Nd_{1.95}Sr_{0.05}CuO_4$ nanofibers by the electrospinning technique, and the resulting SOFC cathode exhibited much reduced polarization resistance compared to the powder cathode [16]. All these results show that one-dimensional nanostructured materials such as nanofibers have great promise as electrode materials for intermediate temperature SOFCs.

In this work, MIEC nanofibers composed of lanthanum strontium nickel oxide ($La_{1.6}Sr_{0.4}NiO_4$, so called LSN) with the K_2NiF_4-type structure were fabricated by the electrospinning technique and tested as SOFC cathode. The electrochemical properties and the kinetics of oxygen reduction on these LSN nanofiber cathodes were studied in detail.

2. Experimental

The $La_{1.6}Sr_{0.4}NiO_4$ (LSN) nanofibers were prepared by electrospinning method. At first, 10 wt.% polyvinylpyrrolidone (PVP) solution was prepared by dissolving PVP in ethanol, to which stoichiometric amounts of $La(NO_3)_3$, $Sr(NO_3)_2$ and $Ni(NO_3)_2$ were added, together with some de-ionized water. Then, the mixture was homogenized for 12 h using a magnetic stirrer to obtain a transparent hybrid sol. The total weight percentage of metal salts was about 3 wt.% in the sol. The hybrid sol was kept static for 10 h to remove the bubbles that occurred during stirring, and then loaded into a syringe for electrospinning experiments. The distance between the spinneret (a metallic needle) and the collector (a grounded plate covered with an aluminum foil) was fixed at 25 cm and the high-voltage supply was maintained at 20 kV. A syringe pump was used to disperse the solution at a spinning rate 5 mL h^{-1}. Then, the as-prepared hybrid fiber precursors were dried at 80 °C in vacuum for 12 h, then heated up to 400 °C at a rate of 5 °C min^{-1}, held for 1 h, and then sintered up to 800 °C at a rate of 1 °C min^{-1} and held for 2 h in air to obtain LSN oxide nanofibers.

These LSN nanofibers were then mixed with terpineol to form ink, which was subsequently painted on one side of the CGO electrolyte to form the working electrode (WE). Platinum paste was painted on the other side of the CGO pellet in symmetric configuration, as the counter electrode (CE). A Pt wire was used as reference electrode (RE) stuck on the same side than the working electrode. Fig. 1 shows the schematic representation of the cell. The cathodes were first heated at 400 °C for 2 h to eliminate organic binders, followed by sintering at 900 °C for 15 min in air, according to the modified "fast firing" method [9]. In this way, LSN nanofiber cathode had a good adhesion to CGO electrolyte while the fiber morphology was retained.

The structure and phase stability of the material were investigated by X-ray powder diffraction using a Bruker D8-Advance diffractometer (operating at 20 kV and 40 mA; Cu Kα radiation with $\lambda = 0.15418$ nm). The diffraction angle was varied from 20 to 80° with a step size of 0.02°. The morphology and microstructure of

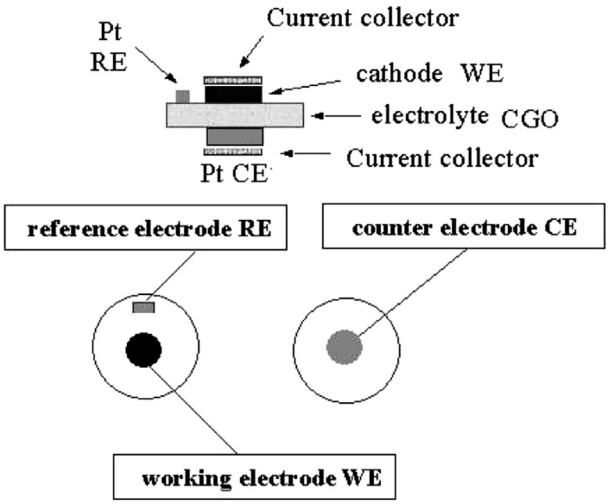

Fig. 1. Schematic representation of the cell.

the sintered electrodes were examined by field emission scanning electron microscope (FEG-SEM, Hitachi S-4700) at an accelerating potential of 10 kV, to obtain secondary electron images. The electrochemical impedance spectroscopy (EIS) diagrams were recorded using an Autolab PGStat30 in the frequency range 1 MHz–0.1 Hz. The measurements were performed at dc = 0 as a function of temperature (500–700 °C) and of oxygen partial pressure (10^{-4}–10^{-1} atm in O_2/N_2 gas mixtures).

3. Results and discussion

Fig. 2(a) shows the SEM image of PVP/LSN nanofibers prior to calcinations. The fibers are uniform in diameter, about 1 μm, and exhibit smooth surface due to the amorphous nature of the polymer. Their surface becomes coarse and the diameter shrinks to 400–500 nm after the calcination at 800 °C for 2 h, due to burning out of the PVP organic components and to the crystallization of LSN material (Fig. 2(b)). The XRD pattern (inset in Fig. 2(b)) indicates that all diffraction peaks characterize the K_2NiF_4-type structure of LSN (JCPDS-89-0425) material, which is in agreement with previous results [17].

It is well known that a significant grain growth leads to agglomeration phenomenon of nanomaterials above 1000 °C [8]. In this report, a fast-firing process with rapid heating as well as short dwell time was intentionally chosen, aiming to suppress the grain growth and to retain the nanofiber structure. Fig. 2(c) and (d) shows images of the surface and cross-section microstructures of LSN nanofiber cathode sintered on CGO electrolyte at 900 °C for 15 min, respectively. The LSN nanofiber cathode exhibits porous hollow structure. The diameter of LSN nanofibers is about 500 nm and is composed of ~50 nm LSN particles, which are slightly larger than that of the raw fibers before sintering. Large pores at micron scale were observed within the nanofibers network (inset in Fig. 2(c)). For example, given the LSN loading of 5 mg cm^{-2}, the porosity of the cathode (P) was calculated using the following relation [14]

$$P = 1 - \frac{m}{A \times L \times \rho} \quad (1)$$

where m is the cathode mass, A and L are the cathode area and thickness, and ρ is the theoretical density of LSN (~7 g cm^{-3}). The cathode porosity was estimated to be 65%, which reveals that a highly porous cathode was successfully fabricated without addition of any poreformer. From the cross-section image (Fig. 2(d)), it can

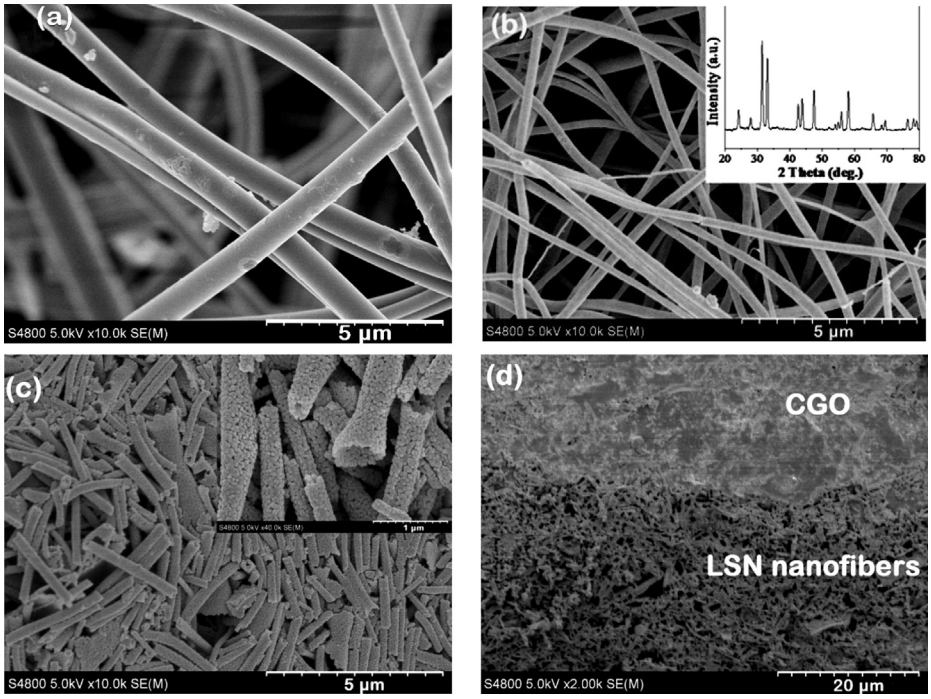

Fig. 2. SEM images of: (a) PVP/LSN composite fibers; (b) fibers calcined at 800 °C (the inset shows the X-ray diagram); (c) LSN nanofiber cathode supported on CGO electrolyte surface; (d) cross-section image after sintering at 900 °C for 15 min.

be seen that the LSN nanofiber cathode with thickness of about 20 μm has good contact with the CGO electrolyte, which is important for the cell performance. Consequently, the results indicate that a rapid sintering strategy at high temperature seems to provide good balance between the conflicting requirements of maintaining a porous, relatively high surface-area fiber cathode on one side, and a good adhesion of the cathode to the electrolyte surface on the other side. This kind of microstructure should be beneficial for improving the cathode property.

Fig. 3 shows typical EIS diagrams of the LSN nanofiber cathode measured in the temperature range of 600–700 °C in air. They are composed of a large arc located in between the high frequency and low frequency zones, respectively. These Nyquist plots have been fitted by means of the Zview™ software (Scribner Associates, Inc.), using an equivalent circuit (inset in Fig. 3) constituted of one resistance R_{el} and two R-CPE elements in parallel associated in series. In this equivalent circuit, R_{el} represents the intercept value in the impedance diagram at high frequency side with the real axis: it corresponds to the ohmic resistance of the electrolyte and lead wires. R_H and R_L are the resistances corresponding to the high frequency and low frequency arcs, respectively. The cathode polarization resistance (R_p) of the LSN cathode is the sum of R_H and R_L. CPE is constant phase element whose value reflects the reaction mechanism of different electrode processes. Its impedance can be expressed as: $Z_{CPE} = 1/Y_0(j\omega)^p$, where Y_0 is the module of the CPE element, ω angular frequency and p is a fitting parameter between 0 and 1 related to the depression angle of the semi-circle ($p = 1$ corresponds to a pure capacitance). The value of the equivalent capacitance, C_{eq}, is deduced from the relationship: $C_{eq} = R^{(1-p/p)} \times Y_0^{1/p}$.

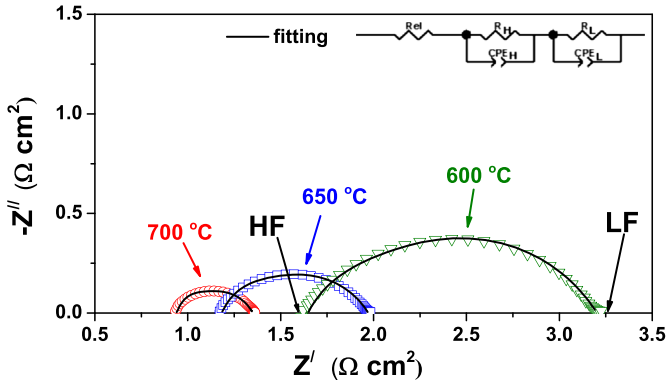

Fig. 3. Impedance diagrams of LSN nanofiber cathode measured in air in between 600 and 700 °C. The inset shows the equivalent circuit used for fitting the data.

From the impedance diagrams (Fig. 3), it can be observed that the value of the polarization resistance (R_p) decreases with temperature. The (R_p) values are: 0.40, 0.80 and 1.59 Ω cm^2 at 700 °C, 650 °C and 600 °C, respectively. These values are lower than these of most nickelate-based conventional powder cathodes reported in the literature [18,19], as well as the one recently reported for the LSM50/YSZ nanofiber composite cathode (0.48 Ω cm^2 at 700 °C in air [20]). One of the main reasons is that the nanofiber cathode is highly porous and percolating; therefore, the surface area of the cathode exposed to oxygen gas is much increased resulting in an increase of the number of electroactive sites for the oxygen reduction reaction (ORR), which promotes the charge transfer ability and reduces the total polarization resistance of the cathode. In addition, it offers a highway for the transport of both electrons and oxide ions [21].

Fig. 4 shows the Arrhenius plot of the polarization resistance (R_p) values for LSN nanofiber cathode. The activation energy (E_a) calculated from the slope of the linear variation is 107.23 kJ mol^{-1}. This value is lower than those of the other K_2NiF_4-type powder cathodes [22,23], *e.g.* E_a = 156.49 kJ mol^{-1} for $Nd_2NiO_{4+\delta}$ and E_a = 124.07 kJ mol^{-1} for $Pr_2NiO_{4+\delta}$. This reduced activation energy could improve the cathode efficiency at intermediate temperature.

In order to determine the reaction rate limiting step, the effect of oxygen partial pressure on the polarization resistance of LSN nanofibers cathode was further studied. Fig. 5(a) shows typical

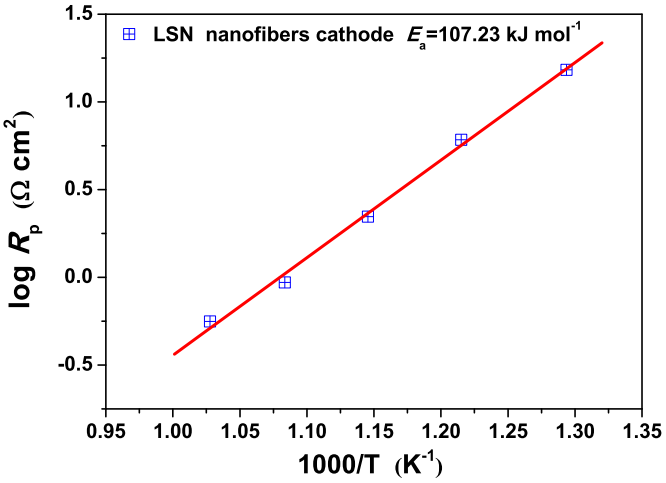

Fig. 4. Arrhenius plot of the polarization resistance of LSN nanofiber cathode in air.

impedance diagrams measured at 700 °C under different oxygen partial pressures (pO_2). Two characteristics of these EIS diagrams are readily noticeable. First, the polarization resistance (R_p) becomes larger with the decrease of pO_2, indicating an influence of the oxygen concentration on the ORR process. Secondly, all the impedance diagrams are fitted using two arcs located at high frequency and low frequency zones, implying the polarization resistance mainly comes from two different electrode processes. The oxygen partial pressure dependence of R_p for LSN nanofiber cathode in the range 600–700 °C is shown in Fig. 5(b); from the linear variation of the pO_2 dependence, the slope can be calculated.

Generally, R_p varies with the oxygen partial pressure according to the following equation (2):

$$R_p = R_p^0 \times (pO_2)^{-n} \quad (2)$$

where R_p^0 is the polarization resistance, the n value characterizing the rate determining step as follows:

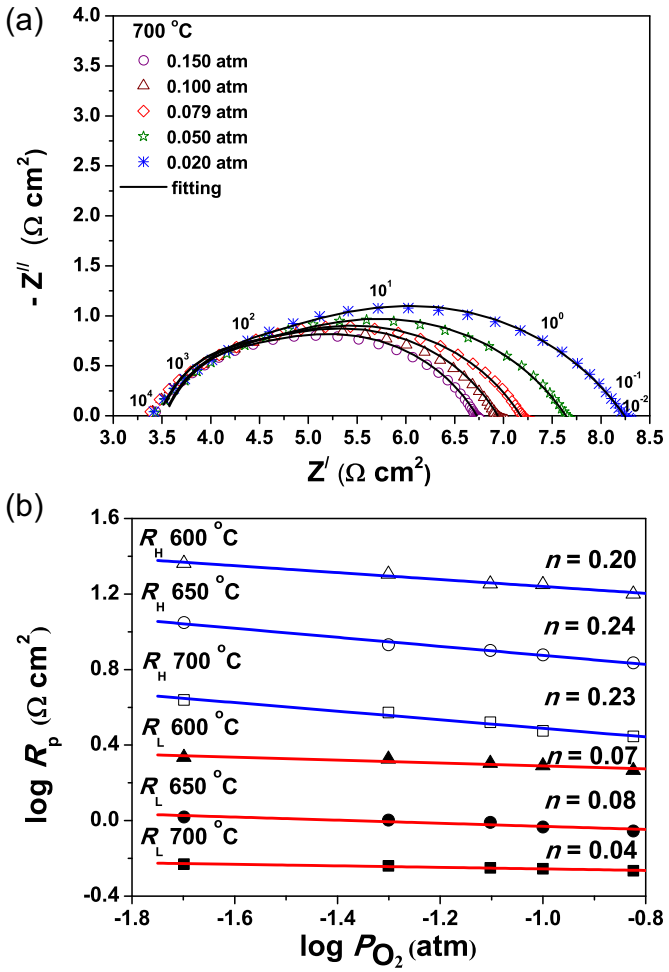

Fig. 5. (a) Impedance diagrams of LSN nanofiber cathode at 700 °C under various oxygen partial pressures. (b) Oxygen partial pressure dependence of R_H and R_L of LSN nanofiber cathode at 700 °C.

$n = 1$, $O_2(g) \Leftrightarrow O_{2,ads.}$
(characterizes the molecular oxygen diffusion and adsorption at the electrode surface sites)
$n = 1/2$, $O_{2,ads.} \Leftrightarrow 2O_{ads.}$
(related to the dissociation of the adsorbed molecular oxygen and surface diffusion)
$n = 1/4$, $O_{ads.} + 2e^- + V_O^{\cdot\cdot} \Leftrightarrow O_O^x$
(corresponds to the electronic transfer at the gas/electrode interface and the subsequent formation of oxide anions)
$n = 0$, $O^{2-}_{(electrode)} \Leftrightarrow O^{2-}_{(electrolyte)}$
(characterizes the ionic transfer of O^{2-} oxide ions across the electrolyte–electrode interface)

Therefore, the value of n may give useful information about the rate determining step of the ORR [24,25]. In a previous study, the $p(O_2)^{-1/4}$ relationship was considered as the contribution of the charge transfer process on the electrode, which was observed for K_2NiF_4-type cathode materials, such as $Ln_2NiO_{4+\delta}$ [26,27]. The $p(O_2)^0$ relationship has been observed for $La_2Cu_{1-x}Co_xO_4$ and $Sr_{1.5}La_xMnO_4$ cathode materials [28,29]. It was assigned to the oxide ion transfer into the electrolyte.

According to Fig. 5(b), the observed n value is around 0 for R_L and 0.25 for R_H, respectively. Considering the weak dependence of R_L on oxygen partial pressure, we propose that the low frequency arc is assigned to be the oxide ion transfer from the TPB to CGO electrolyte; whereas the high frequency arc is due to the charge transfer process at the electrode surface. With regards to the results of Fig. 5(b), it is also observed that R_H is always larger than R_L in the whole range of oxygen partial pressures from 600 to 700 °C. Therefore, it is concluded that the charge transfer process is the major rate limiting step for LSN nanofiber cathode.

The exchange current density, i_0, which reflects the intrinsic oxygen reduction reaction rate, is an important parameter to investigate the ORR mechanism at the cathode [30]. The i_0 value can be obtained from the impedance measurement. In this

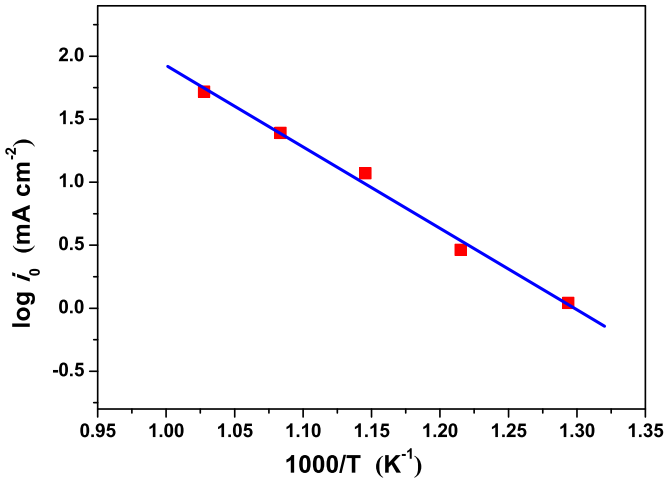

Fig. 6. Arrhenius plot of the exchange current density i_0 for LSN nanofiber cathode.

technique, i_0 was calculated from the polarization resistance, R_p of the Nyquist plot using equation (3) which is derived from the Butler–Volmer equation [31]:

$$i_0 = \frac{RTv}{nFR_p} \quad (3)$$

where R is the gas constant, T the temperature in Kelvin, v is the number of times the rate limiting step occurs for one occurrence of the full reaction, n is the total number of electrons transferred in the reaction and F the Faraday constant. For the ORR, n and v are generally assumed to be 4 and 1, respectively (as the total number of transferred electrons transferred per reduced molecule of oxygen is 4 and the rate limiting step would likely have a stoichiometry of 1 for the ORR) [32].

The variation of i_0 values as a function of inverse temperature is shown in Fig. 6. The linearity of this Arrhenius plot indicates that the cathode is stable as a function of temperature. It is also observed that the i_0 values rapidly increase with the increasing operating temperature. The i_0 value reaches 52.4 mA cm^{-2} at 700 °C in air, which is higher than those of $La_{1.6}Sr_{0.4}NiO_4$ and $La_2NiO_{4+\delta}$ powder cathodes [33,19]. This is understandable, considering the well constructed microstructure of the nanofiber cathode which promotes the surface diffusion or adsorption process. Furthermore, in the one-dimensional fiber cathode, a continuous electrode network is formed, which likely supplies a highway for oxide ion transport and an uninterrupted path that facilitates the gas-phase diffusion and charge transport. As a result, the number of electrochemical active sites is efficiently extended throughout the whole electrode and the ORR is enhanced.

4. Conclusions

K_2NiF_4-type nanofiber oxide $La_{1.6}Sr_{0.4}NiO_4$ (LSN) has been prepared for the first time and studied as cathode material for SOFCs based on ceria electrolyte. The results show that the nanofiber architecture can be stabilized at intermediate operating temperatures after a rapid sintering at 900 °C for 15 min in air. The LSN nanofiber cathode is highly porous but forms good contact with the CGO electrolyte. The rate limiting step for the ORR on LSN nanofiber electrode is the charge transfer process. The polarization resistance obtained at 700 °C in air is about 0.40 Ω cm^2 and the exchange current density i_0 is 52.4 mA cm^{-2}. Compared to results obtained for usual powder electrodes, the present work shows that the performance of the intermediate temperature SOFCs may be improved by engineering the electrode architecture at the nanoscale.

Acknowledgments

The Project was supported by National Natural Science Foundation of China (51102083, 51302069, 51372073), Program for New Century Excellent Talents in University (NCET-13-0779), Youth Scholar Backbone Supporting Plan Project of Heilongjiang General Colleges and Universities (1253G046), Natural Science Foundation of Heilongjiang Province (JC201211, B201107).

References

[1] D. Brett, A. Atkinson, N.P. Brandon, S.J. Skinner, Chem. Soc. Rev. 37 (2008) 1568–1578.
[2] M. Tsuchiya, B.K. Lai, S. Ramanathan, Nat. Nanotechnol. 6 (2011) 282–286.
[3] W. Zhou, L. Ge, Z.G. Chen, F.L. Liang, H.Y. Xu, J. Motuzas, A. Julbe, Z.H. Zhu, Chem. Mater. 23 (2011) 4193–4198.
[4] L.M. Acuña, J. Peña-Martínez, D. Marrero-López, R.O. Fuentes, P. Nuñez, D.G. Lamas, J. Power Sources 196 (2011) 9276–9283.
[5] B. Liu, X.B. Chen, Y.L. Dong, S.S. Mao, M.J. Cheng, Adv. Energy Mater. 1 (2011) 343–346.
[6] J. Choi, B. Kim, D. Shin, J. Eur. Ceram. Soc. 33 (2013) 2269–2273.
[7] N.Q. Zhang, J. Li, W. Li, D. Ni, K.N. Sun, RSC Adv. 2 (2012) 802–804.
[8] M.G. Bellino, J. Sacanell, D.G. Lamas, A.G. Leyva, N.E. Walsöe de Reca, J. Am. Chem. Soc. 129 (2007) 3066–3067.
[9] J. Sacanell, A.G. Leyva, M.G. Bellino, D.G. Lamas, J. Power Sources 195 (2010) 1786–1792.
[10] D.H. Dong, Y.Z. Wu, X.Y. Zhang, J.F. Yao, Y. Huang, D. Li, C.Z. Li, H.T. Wang, J. Mater. Chem. 21 (2011) 1028–1032.
[11] D.H. Dong, J.F. Yao, Y.Z. Wu, X.Y. Zhang, G.S. Xu, C.Z. Li, H.T. Wang, Electrochem. Commun. 13 (2011) 1038–1041.
[12] A. Greiner, J.H. Wendorff, Angew. Chem. Int. Ed. 46 (2007) 5670–5703.
[13] M.J. Zhi, N. Mariani, R. Gemmen, K. Gerdesa, N.Q. Wu, Energy Environ. Sci. 4 (2011) 417–420.
[14] M.J. Zhi, S. Lee, N. Miller, N.H. Menzler, N.Q. Wu, Energy Environ. Sci. 5 (2012) 7066–7071.
[15] X.N. Jiang, H.X. Xu, Q. Wang, L. Jiang, X.N. Li, Q.L. Xu, Y.C. Shi, Q.Y. Zhang, J. Alloys Compd. 557 (2013) 184–189.
[16] L.P. Sun, Q. Li, H. Zhao, L.H. Huo, J.H. Hao, G.S. Pang, Z. Shi, S.H. Feng, Int. J. Hydrogen Energy 37 (2012) 11955–11962.
[17] M. Jamest, J. Paul Attfield, J. Mater. Chem. 6 (1996) 57–62.
[18] Q. Li, Y. Fan, H. Zhao, L.P. Sun, L.H. Huo, J. Power Sources 167 (2007) 64–68.
[19] H. Zhao, F. Mauvy, C. Lalanne, J.M. Bassat, S. Fourcade, J.C. Grenier, Solid State Ionics 179 (2008) 2000–2005.
[20] N.Q. Zhang, J. Li, Z.L. He, K.N. Sun, Electrochem. Commun. 13 (2011) 570–573.
[21] J.M. Vohs, R.J. Gorte, Adv. Mater. 21 (2009) 943–956.
[22] F. Mauvy, J.M. Bassat, E. Boehm, J.P. Manaud, P. Dordor, J.C. Grenier, Solid State Ionics 158 (2003) 17–28.
[23] C. Ferchaud, J.C. Grenier, Y. Zhang-Steenwinkel, M.M.A. van Tuel, F.P.F. van Berkel, J.M. Bassat, J. Power Sources 196 (2011) 1872–1879.
[24] R.A. Souza, J.A. Kilner, Solid State Ionics 106 (1998) 175–187.
[25] R.A. Souza, J.A. Kilner, Solid State Ionics 126 (1999) 153–161.
[26] L.P. Sun, Q. Li, H. Zhao, L.H. Huo, J.C. Grenier, J. Power Sources 183 (2008) 43–48.
[27] F. Mauvy, C. Lalanne, J.M. Bassat, J.C. Grenier, H. Zhao, L. Huo, P. Stevens, J. Electrochem. Soc. 153 (8) (2006) A1547–A1553.
[28] Q. Li, X. Zeng, L.P. Sun, H. Zhao, L.H. Huo, J.C. Grenier, Int. J. Hydrogen Energy 37 (2012) 2552–2558.
[29] L.P. Sun, Q. Li, L.H. Huo, H. Zhao, G.Y. Zhang, N. Lin, J.P. Viricelle, C. Pijolat, J. Power Sources 196 (2011) 5835–5839.
[30] S.B. Adler, Chem. Rev. 104 (2004) 4791–4843.
[31] Y.P. Fu, Int. J. Hydrogen Energy 35 (2010) 8663–8669.
[32] J. Liu, A.C. Co, B. Paulson, V.I. Briss, Solid State Ionics 177 (2006) 377–387.
[33] Q. Li, Y. Fan, H. Zhao, L.H. Huo, Chin. J. Inorg. Chem. 22 (2006) 2025–2030.